Electronic Supporting Information

Signatures of a Quantum Diffusion Limited Hydrogen Atom Tunneling Reaction

Morgan E. Balabanoff, Mahmut Ruzi, and David T. Anderson*

Department of Chemistry, University of Wyoming, Laramie, WY 82071

***Email: danderso@uwyo.edu**

Table S1. Species, assigned mode, measured peak position, integrated absorption coefficient and integration limits used to determine concentrations.

Species	Mode	ν (cm^{-1})	ε (km mol^{-1})	Limits (cm^{-1})	Ref.
CH_3OH	ν_1 (OH)	3672.80	43.1	3660.0 – 3690.0	[1]
CH_3OH	ν_3 (CH sym)	2840.70	38.8	2830.0 – 2860.0	[1]
CH_3OH	ν_5 (CH_3 rock)	1449.16	1.6	1447.0 – 1452.0	[1]
CD_3OH	ν_1 (OH)	3672.48	45	3660.0 – 3690.0	[2]
CD_3OH	ν_5 (CD_3 sym bend)	1127.68	64	1120.0 – 1129.5	[2]
CD_3OD	ν_4 (CD_3 sym bend)	1132.06	42	1129.5 – 1138	[2]
CH_2OH	ν_6 (CO)	1179.33	104	1178.5 – 1180.0	[3]
CD_2OH	ν_6 (CO)	1212.84	124	1211.0 – 1215.0	This work
CD_2OD	ν_6 (CO)	1219.70	87	1218.5 – 1221.0	This work
CH_2O	ν_1 (CH sym)	2782.42	61.7	2780.0 – 2788.0	[4]
CH_2O	ν_2 (CO str)	1742.60	74	1741.0 – 1744.0	[4]
CH_2O	ν_3 (HCH bend)	1497.72	11.2	1497.0 – 1499.0	[4]
CH_2O	$2\nu_2$ (CO str)	3465.00	3.8	3464 – 3466	[4]
CHDO	ν_2 (CO str)	1720.78	69.3	1720.0 – 1721.5	[5]
CD_2O	ν_2 (CO str)	1698.04	58.4	1697.5 – 1698.5	[5]
H_2O	ν_3 (asym stretch)	3765.45	53.6	3764.5 – 3766.75	[6]
CHO	ν_2 (CO str)	1864.77	70	1864.0 – 1865.5	[7]
CO	ν_{CO}	2142.95	46.8	2130 - 2150	[7]

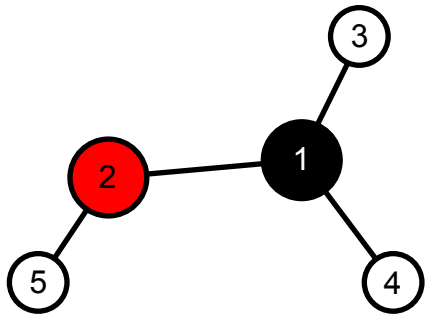

Figure S1. CH_2OH atom designations used in Table S2.

Table S2. Fully optimized geometry parameters for the CH_2OH radical. Distances in Å, angles in degrees, and energy in Hartree (with ZPE correction).

Geometry	MP2[a]	MP2[b]	B3PW91[a]	B3PW91[b]	B3LYP[b]
Energy	-114.817629	-114.828514	-115.030409	-115.062250	-115.077137
R(1,2)	1.365	1.367	1.36	1.373	1.365
R(1,3)	1.075	1.075	1.079	1.085	1.077
R(1,4)	1.079	1.079	1.082	1.088	1.081
R(2,5)	0.960	0.962	0.960	0.970	0.962
A(2,1,3)	113.282	113.322	114.027	113.742	113.935
A(2,1,4)	118.684	118.638	119.243	119.273	119.143
A(3,1,4)	120.653	121.101	121.621	121.814	121.844
A(1,2,5)	108.356	108.966	109.758	109.138	110.069
D(3,1,2,5)	174.613	174.499	175.488	175.092	175.318
D(4,1,2,5)	24.375	23.296	20.331	20.030	20.033

[a]cc-pVTZ basis
[b]aug-cc-pVTZ basis
ip – in phase, oop – out of phase, tor - torsion

Table S3. Vibrational frequencies (cm^{-1}) and IR intensity (km/mol) for CH_2OH radical.

assignment	MP2[a]	MP2[b]	B3PW91[a]	B3PW91[b]	B3LYP[b]
ν(O-H)	3880.1(69)	3856.9(74)	3855.3(63)	3719.7(49)	3823.0(62)
ν_a(C-H)	3340.9(10)	3342.8(6)	3279.2(9)	3210.4(10)	3273.5(9)
ν_s(C-H)	3190.8(20)	3193.0(20)	3138.3(19)	3071.0(19)	3133.6(18)
CH_2 scis	1517.3(9)	1509.0(9)	1478.6(9)	1436.4(7)	1481.8(8)
ip HCOH bend	1381.5(24)	1367.8(23)	1357.3(26)	1326.3(23)	1356.0(29)
ν(C-O)	1224.7(104)	1212.6(118)	1218.0(111)	1167.3(96)	1198.8(109)
oop HCOH bend	1074.2(50)	1067.3(50)	1050.9(47)	1022.1(47)	1052.1(47)
CH_2 wag	646.8(69)	623.5(75)	525.1(119)	508.9(126)	524.5(121)
HCOH tor	439.8(71)	433.2(61)	406.9(28)	404.9(16)	410.3(25)

[a]cc-pVTZ basis
[b]aug-cc-pVTZ basis
ip – in phase, oop – out of phase, tor - torsion

Table S4. Vibrational frequencies (cm^{-1}) and IR intensity (km/mol) for CD_2OD radical.

assignment	MP2[a]	MP2[b]	B3PW91[a]	B3PW91[b]	B3LYP[b]
ν(O-D)	2825.1(42)	2808.4(46)	2807.1(39)	2708.3(30)	2783.6(39)
ν_a(C-D)	2497.2(7)	2499.2(5)	2451.9(6)	2400.5(7)	2448.0(6)
ν_s(C-D)	2306.8(20)	2307.5(20)	2268.3(19)	2218.4(18)	2263.8(18)
ν(C-O)+CD_2 scis	1268.3(80)	1251.9(94)	1252.6(88)	1200.6(75)	1235.0(87)
ip DCOD bend	1070.4(25)	1061.8(26)	1054.1(27)	1027.4(22)	1053.8(28)
CD_2 scis + ν(C-O)	1047.7(14)	1043.8(14)	1026.8(11)	998.8(14)	1026.9(13)
oop DCOD bend	778.6(24)	773.2(24)	762.6(24)	742.5(22)	763.2(23)
CD_2 wag	506.33(33)	487.5(36)	405.0(57)	389.7(61)	403.6(58)
DCOD tor	322.8(44)	318.5(39)	303.7(24)	304.1(17)	306.8(23)

[a]cc-pVTZ basis
[b]aug-cc-pVTZ basis
ip – in phase, oop – out of phase, tor - torsion

Table S5. Vibrational frequencies (cm^{-1}) and IR intensity (km/mol) for CH_2OD radical.

assignment	MP2[a]	MP2[b]	B3PW91[a]	B3PW91[b]	B3LYP[b]
ν_a(C-H)	3341.3(9)	3343.2(5)	3279.7(8)	3211.0(9)	3274.0(8)
ν_s(C-H)	3190.8(20)	3193.0(20)	3138.3(19)	3071.0(19)	3133.6(18)
ν(O-D)	2824.7(44)	2808.0(47)	2806.7(40)	2707.7(31)	2783.2(40)
CH_2 scis	1517.2(8)	1508.7(8)	1478.4(8)	1436.1(6)	1481.6(7)
ip HCOD bend	1254.2(4)	1245.4(5)	1227.3(5)	1195.1(3)	1227.7(5)
ν(C-O)	1222.9(100)	1210.5(116)	1216.0(106)	1165.6(94)	1196.6(107)
oop HCOD bend	876.1(38)	868.3(36)	860.9(37)	840.0(36)	861.1(37)
CH_2 wag	643.8(55)	619.8(58)	513.5(80)	493.2(83)	511.7(80)
HCOD tor	363.4(36)	358.4(31)	342.0(19)	343.6(14)	345.7(19)

See Table S4 for abbreviations

Table S6. Vibrational frequencies (cm^{-1}) and IR intensity (km/mol) for CD_2OH radical.

assignment	MP2[a]	MP2[b]	B3PW91[a]	B3PW91[b]	B3LYP[b]
ν(O-H)	3879.9(70)	3856.6(75)	3855.1(64)	3719.5(49)	3822.8(63)
ν_a(C-D)	2497.8(7)	2499.8(4)	2452.5(6)	2401.2(7)	2448.6(6)
ν_s(C-D)	2306.8(20)	2307.5(20)	2268.4(19)	2218.5(18)	2263.8(18)
ip DCOH bend	1322.5(16)	1306.6(18)	1302.3(16)	1273.1(21)	1298.4(27)
ν(C-O) + CD_2 scis	1261.6(126)	1247.8(135)	1246.9(136)	1194.8(113)	1232.0(124)
CD_2 scis + ν(C-O)	1049.3(20)	1045.8(22)	1028.9(17)	1000.0(17)	1029.2(19)
oop DCOH bend	861.0(18)	856.3(18)	842.1(17)	818.4(16)	843.0(17)
CD_2 wag	511.0(55)	493.6(63)	430.8(123)	425.6(124)	432.7(125)
DCOH tor	405.8(76)	399.1(63)	362.3(10)	353.0(3)	363.1(7)

See Table S4 for abbreviations

Table S7. Vibrational frequencies (cm^{-1}) and IR intensity (km/mol) for *trans*-CHDOH radical.

assignment	MP2[a]	MP2[b]	B3PW91[a]	B3PW91[b]	B3LYP[b]
ν(O-H)	3880.1(69)	3856.8(74)	3855.3(63)	3719.6(49)	3822.9(62)
ν(C-H)	3298.6(10)	3299.1(8)	3238.9(9)	3171.5(9)	3233.4(8)
ν(C-D)	2376.3(18)	2379.0(16)	2336.7(17)	2285.6(17)	2332.7(17)
oop HCOH bend	1422.0(27)	1412.7(26)	1390.6(31)	1354.9(25)	1392.4(30)
COH bend	1330.2(3)	1312.2(4)	1308.4(5)	1271.2(3)	1299.6(4)
ip HCOH bend	1182.3(141)	1172.8(154)	1171.1(142)	1126.0(131)	1160.7(146)
oop HCOD bend	919.8(14)	915.8(12)	898.3(12)	873.4(11)	899.0(12)
HCO tor	597.6(72)	579.1(79)	505.4(120)	495.1(123)	506.5(122)
DCOH tor	409.1(62)	401.3(52)	364.6(19)	358.3(10)	366.3(16)

[a]cc-pVTZ basis
[b]aug-cc-pVTZ basis
ip – in phase, oop – out of phase, tor - torsion

Table S8. Vibrational frequencies (cm^{-1}) and IR intensity (km/mol) for *cis*-CHDOH radical.

assignment	MP2[a]	MP2[b]	B3PW91[a]	B3PW91[b]	B3LYP[b]
ν(O-H)	3880.0(70)	3856.7(75)	3855.2(64)	3719.6(49)	3822.8(63)
ν(C-H)	3247.2(19)	3251.0(16)	3191.7(18)	3122.9(19)	3186.7(17)
ν(C-D)	2414.8(10)	2414.9(10)	2371.8(9)	2321.8(9)	2367.5(9)
ip HCOH bend	1420.7(3)	1410.0(4)	1389.3(3)	1350.0(3)	1389.3(3)
COH bend	1296.8(102)	1286.1(100)	1276.6(114)	1241.3(82)	1274.5(104)
ν(C-O)	1214.8(50)	1203.9(64)	1205.9(46)	1161.4(59)	1189.6(56)
ip DCOH bend	917.4(28)	910.7(29)	893.6(27)	868.7(25)	895.1(27)
HCD tor	572.4(43)	550.4(47)	452.8(91)	435.9(113)	451.2(97)
HOC tor	423.3(94)	418.3(85)	402.9(51)	403.3(23)	407.1(45)

See Table S6 for abbreviations

Table S9. Vibrational frequencies (cm^{-1}) and IR intensity (km/mol) for *trans*-CHDOD radical.

assignment	MP2[a]	MP2[b]	B3PW91[a]	B3PW91[b]	B3LYP[b]
ν(C-H)	3247.3(19)	3251.1(16)	3191.9(18)	3121.1(19)	3186.9(17)
ν(O-D)	2824.9(42)	2808.2(46)	2806.9(39)	2707.9(30)	2783.3(39)
ν(C-D)	2414.4(11)	2414.5(11)	2371.4(10)	2321.3(10)	2367.0(10)
HCO bend	1404.7(13)	1396.6(13)	1372.1(14)	1330.0(10)	1372.5(11)
ν(C-O)	1223.0(98)	1211.7(113)	1215.1(103)	1165.7(93)	1198.3(107)
oop DCOD bend	1069.6(4)	1060.9(3)	1049.7(4)	1025.2(4)	1048.6(4)
ip DCOD bend	824.5(33)	817.1(33)	805.8(32)	784.8(30)	806.7(32)
CHD tor	571.6(38)	549.5(41)	448.9(56)	428.9(59)	446.6(56)
HCO tor	338.4(46)	334.4(42)	324.3(35)	327.3(31)	328.3(35)

See Table S6 for abbreviations

Table S10. Vibrational frequencies (cm^{-1}) and IR intensity (km/mol) for *cis*-CHDOD radical.

assignment	MP2[a]	MP2[b]	B3PW91[a]	B3PW91[b]	B3LYP[b]
ν(C-H)	3298.9(8)	3299.4(7)	3239.3(7)	3171.9(8)	3233.7(7)
ν(O-D)	2824.7(44)	2808.1(47)	2806.8(41)	2707.9(32)	2783.3(40)
ν(C-D)	2376.4(17)	2378.9(16)	2336.5(16)	2285.4(16)	2332.5(16)
HCO bend	1404.6(14)	1394.3(15)	1370.9(17)	1331.2(12)	1371.8(15)
ν(C-O)	1231.7(67)	1217.8(82)	1218.9(71)	1173.2(62)	1202.1(72)
ip DCOD bend	1075.2(42)	1068.0(43)	1058.0(41)	1027.7(41)	1057.4(44)
oop DCOD bend	813.9(26)	808.3(24)	797.1(24)	776.9(23)	797.4(23)
CHD tor	589.5(48)	569.4(51)	482.6(73)	466.9(76)	481.9(74)
DCOD tor	334.7(34)	329.4(30)	308.1(16)	306.9(11)	310.8(15)

[a]cc-pVTZ basis
[b]aug-cc-pVTZ basis
ip – in phase, oop – out of phase, tor - torsion

Table S11. Peak positions for the observed CH_2OH transitions.

Mode	$K_a'\leftarrow K_a''$	B3LYP	gas	pH_2 (Lee)[8,9]	pH_2 (Expt.)
ν_1 (OH)	1←0				3657.62
ν_1 (OH)	0←0	3823(62)	(3674.9)[10]	3651.9	3651.94
ν_2 (CH_2 str)$_a$	0←0	3274(9)	(3161.5)[10]	3165.3	3165.12
ν_3 (CH_2 str)$_s$	0←0	3134(18)	(3041.7563)[11]		3039.37
ν_3 (CH_2 str)$_s$	0←0	3134(18)	(3041.7563)[11]	3038.5	3038.53
ν_4 (CH_2 sci)	0←0	1482(8)		1457.8	1457.76
ν_5 (ip bend)	0←0	1356(29)		1332.1	1332.05
ν_6 (CO str)	0←0	1199(109)	1176(±7)[12]	1179.3	1179.33
ν_7 (oop bend)	0←0	1052(47)		1046.9	1046.97

Table S12. Peak positions for the observed CD_2OH transitions.

Mode	$K_a'\leftarrow K_a''$	B3LYP	Gas	pH_2 (Lee)[8,9]	pH_2 (Expt.)
ν_1 (OH)	1←0				3657.22
ν_1 (OH)	0←0	3823(63)		3653.6	3653.65
ν_1 (OH)	0←0				3653.18
ν_2 (CD_2 str)$_a$	0←0	2449(6)			2430.33
ν_3 (CD_2 str)$_s$	0←0	2264(18)		2197.0	2197.05
ν_4 (CD_2 sci)	0←0	1029(19)	1019(±4)[12]	1017.1	1017.09
ν_5 (ip bend)	0←0	1298(27)		1280.5	1280.6
ν_6 (CO str)	0←0	1232(124)	1208(±10)[12]	1212.9	1212.84
ν_7 (oop bend)	0←0	843(17)		840.7	840.8

Table S13. Peak positions for the observed CD_2OD transitions.

Mode	K_a'←K_a''	B3LYP	Gas	Ar[13,14]	pH_2 (Expt.)
ν_1 (OD)	1←0				2702.08
ν_1 (OD)	0←0	2784(39)		2694	2699.30
ν_2 (CD_2 str)$_a$	0←0	2448(6)			
ν_3 (CD_2 str)$_s$	0←0	2264(18)			2197.79
ν_4 (CD_2 sci)	0←0	1027(13)	1020(±5)[12]		1015.08
ν_5 (ip bend)	0←0	1054(28)		1041	1040.57
ν_6 (CO str)	0←0	1235(87)	1221(±4)[12]	1223	1219.74
ν_7 (oop bend)	0←0	763(23)		765	764

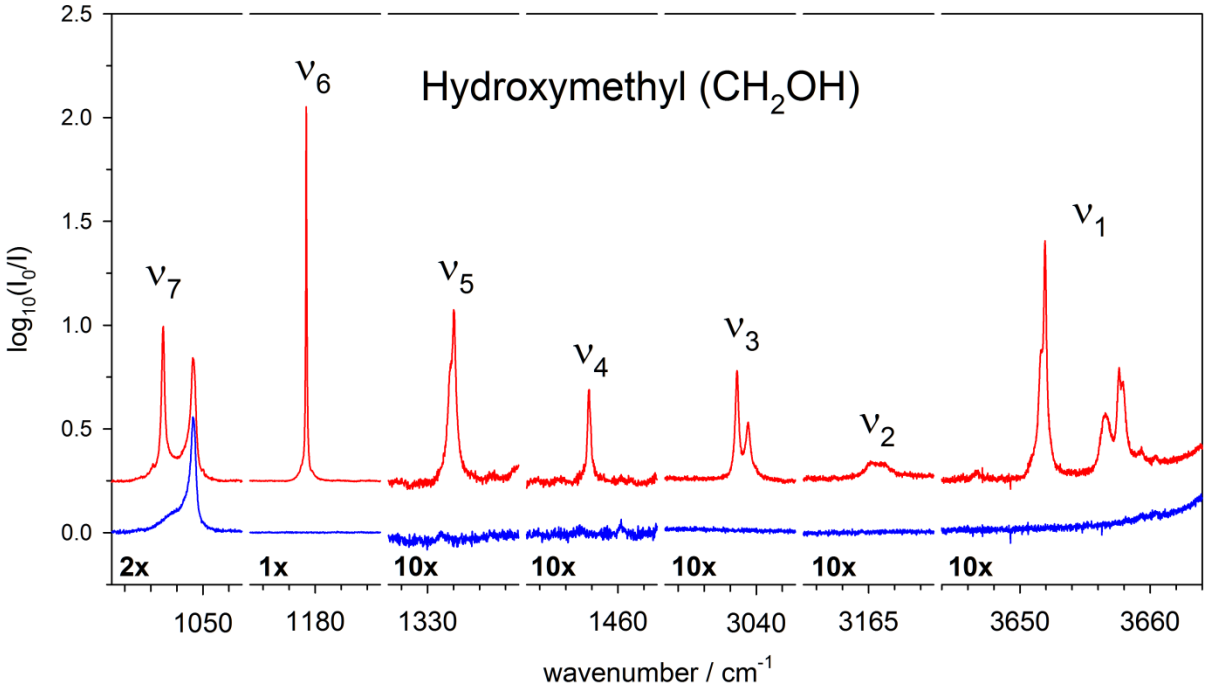

Figure S2. Representative (Expt. #4) infrared spectra in the regions of the peaks assigned to CH_2OH both before (blue) and after (red) the 193 nm photoinduced reaction on a CH_3OH/pH_2 sample. Note the absorption intensity was multiplied by the scale factor indicated at the bottom of each trace. Most peaks are single peaks, but ν_3 and ν_1 show additional fine structure.

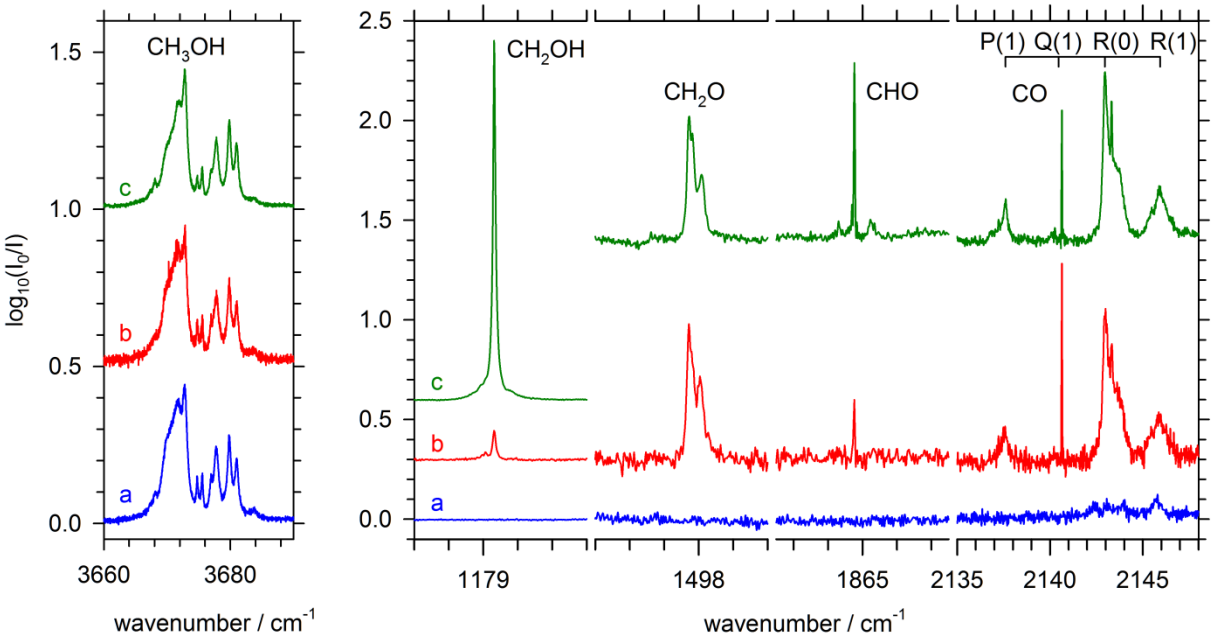

Figure S3. FTIR absorption spectra of CH_3OH, CH_2OH, CH_2O, CHO and CO before and after the photolysis of a CH_3OH/pH_2 sample. Trace (a) is recorded (0.05 cm^{-1} resolution, 16 co-added scans, 3.0 min acquisition time) at 1.84 K before photolysis, trace (b) is recorded 0.38 min after photolysis (3 min, 80 Hz, 56 mW cm^{-2}), and trace (c) is recorded 519.6 min after trace (b) while the sample is maintained at 1.84(1) K.

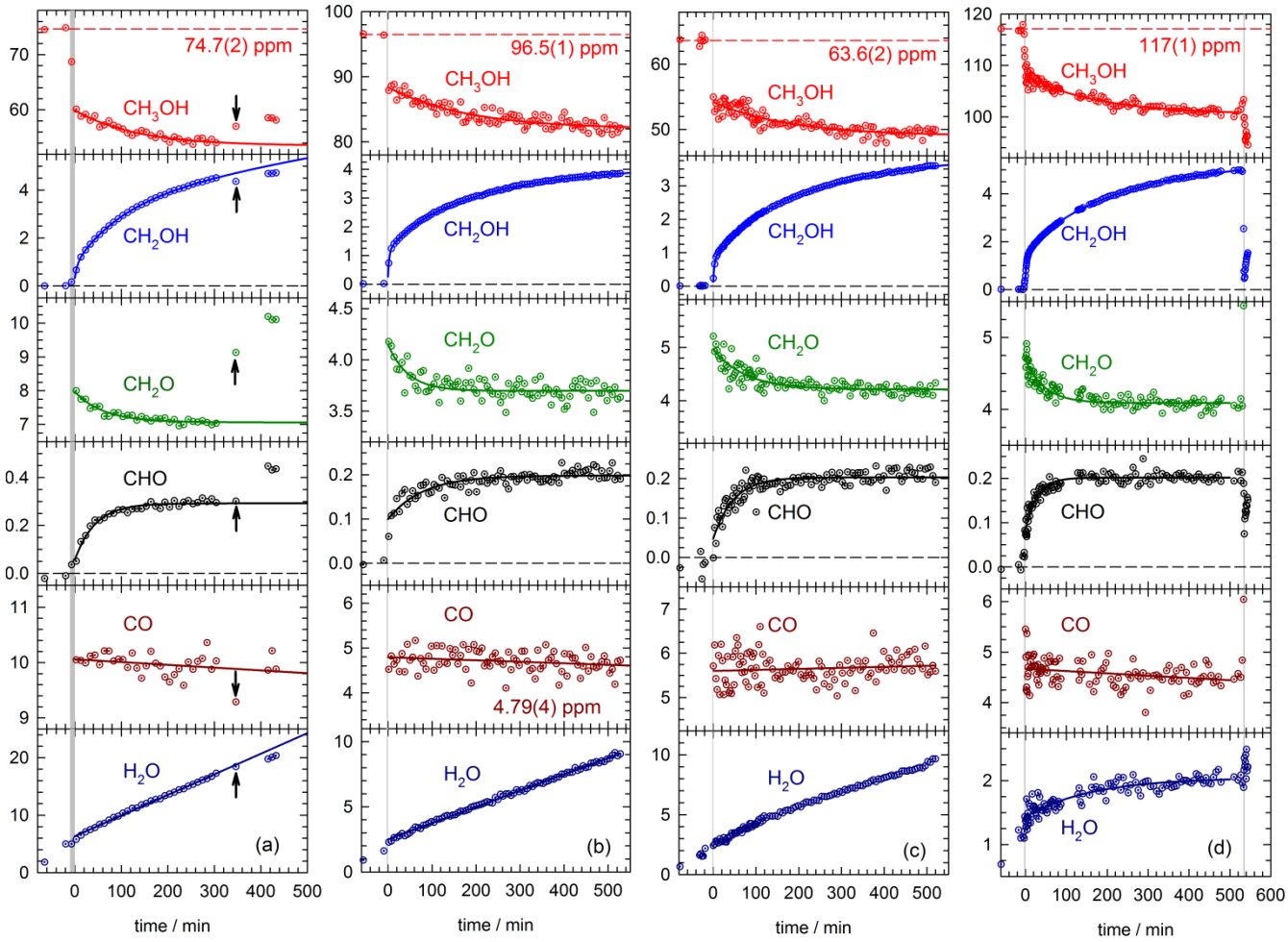

Figure S4. Full kinetic data (concentration in ppm and time in min) for the four low temperature photoinduced chemistry experiments conducted on CH_3OH/pH_2 samples. The conditions are the following: (a) Expt. #1 conducted at 1.89(1) K on an as-deposited sample with 10 min of 14.4 mW cm^{-2} at 40 Hz; arrows indicate raising the temperature to 4.36 K for 20 min and then cooling to 1.73 K and taking 3 more spectra; (b) Expt. #2 conducted at 1.88(1) K on an as-deposited sample with 2.5 min of 25 mW cm^{-2} at 80 Hz; (c) Expt. #3 conducted at 1.88(1) K on an as-deposited sample with 1.66 min of 60 mW cm^{-2} at 240 Hz; (d) Expt. #4 conducted at 1.84(1) K on an as-deposited sample with 3 min of 19 mW cm^{-2} at 80 Hz. At ~533 min a second photolysis was performed with 3 min of 18 mW cm^{-2} at 80 Hz.

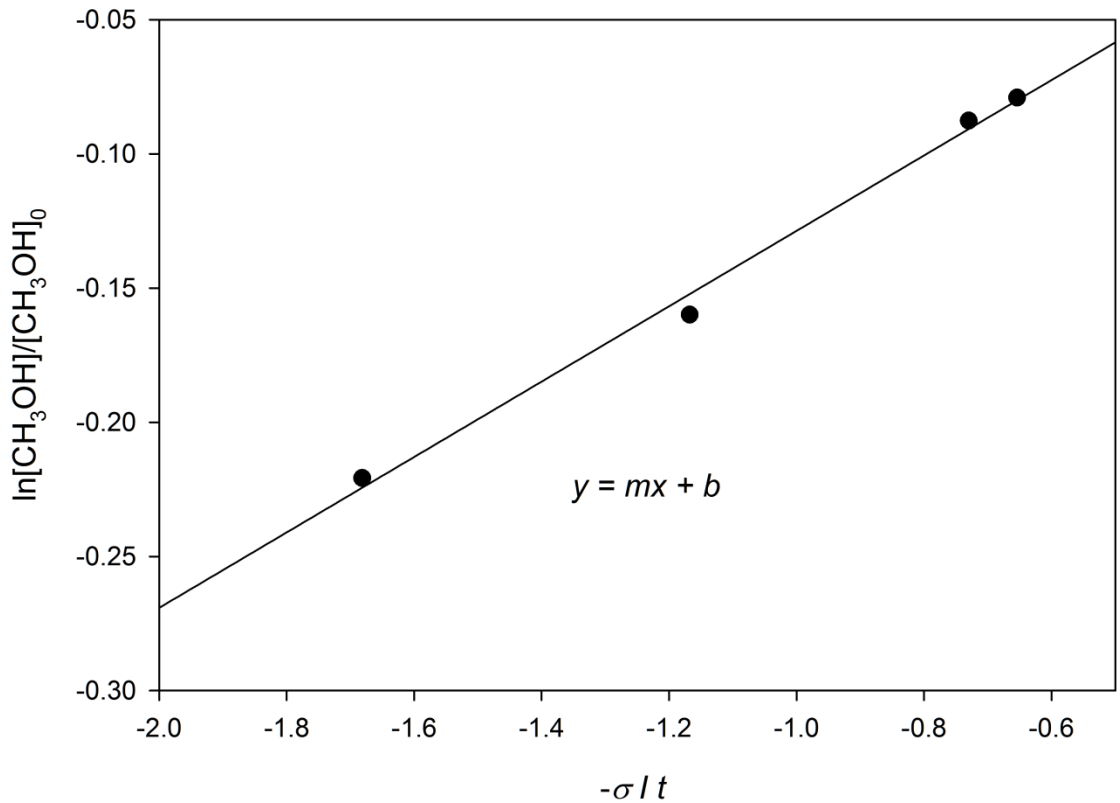

Figure S5. The CH_3OH photolysis data for the four low temperature CH_3OH/pH_2 photolysis experiments are fit to the equation $\ln([CH_3OH]/[CH_3OH]_0) = -\sigma I \Phi\, t$ where σ is the gas-phase cross section at 193 nm ($0.2\text{x}10^{-18}$ cm^2),[15] I is the measured laser fluence (photons cm^{-2} sec^{-1}), t is the photolysis duration in sec, and Φ is the quantum yield. The data was least squares fit to the equation of a line, with m = 0.140(8) and b = 0.012(9).

Table S14. Kinetic parameters for the decay of CH_3OH after photolysis. All concentrations in ppm. The uncertainties in parenthesis represent the 1σ values determined from least-squares fits of the data to Eq. (4).

Expt. #	Expt 1.	Expt. 2	Expt. 3	Expt. 4	Expt. 5
Filename	KAK01061	KAK01069	KAK01080	KAK01135	KAK01145
T / K	1.88	1.88	1.86	1.84	1.74
$[CH_3OH]_\infty$	53.5(5)	82.0(3)	49.0(3)	100.5(3)	103(6)
A	6.4(4)	6.4(3)	5.2(3)	7.6(3)	12(6)
k / 10^{-3} min^{-1}	7.6(1)	5.5(9)	5.5(10)	5.7(7)	3.2(2)
R^2	0.927563	0.821822	0.770651	0.922662	0.640846

Table S15. Kinetic parameters for the decay of CH_2O after photolysis. All concentrations in ppm. The uncertainties in parenthesis represent the 1σ values determined from the least-squares fits of the data to Eq. (4).

Expt. #	Expt 1.	Expt. 2	Expt. 3	Expt. 4	Expt. 5
Filename	KAK01061	KAK01069	KAK01080	KAK01135	KAK01145
T / K	1.89	1.88	1.85	1.84 K	1.74
$[CH_2O]_\infty$	7.07(3)	3.70(1)	4.21(2)	4.09(1)	10.01(6)
A	0.90(6)	0.45(6)	0.76(5)	0.59(3)	0.78(6)
k / 10^{-2} min^{-1}	1.6(2)	2.2(5)	1.3(2)	2.1(3)	1.9(4)
R^2	0.914122	0.504521	0.721	0.829487	0.646366

Table S16. Kinetic parameters for the growth of CHO after photolysis. All concentrations in ppm. The uncertainties in parenthesis represent the 1σ values determined from the least-squares fits of the data to Eq. (5).

Expt. #	Expt 1.	Expt. 2	Expt. 3	Expt. 4	Expt. 5
Filename	KAK01061	KAK01069	KAK01080	KAK01135	KAK01145
T / K	1.89	1.88	1.85	1.84 K	1.74
$[CHO]_0$	0.06(1)	0.099(8)	0.047(9)	0.085(5)	0.128(7)
A	0.24(1)	0.099(7)	0.156(9)	0.117(5)	0.295(7)
k / 10^{-2} min^{-1}	2.3(2)	1.3(2)	2.1(2)	3.5(3)	2.5(1)
R^2	0.954278	0.74028	0.796749	0.888749	0.943899

Table S17. Kinetic parameters for the growth of CH_2OH after photolysis. All concentrations in ppm. The uncertainties in parenthesis represent the 1σ values determined from the least-squares fits of the data to sum of three first-order rate expressions.

	Expt. 1	Expt. 2	Expt. 3	Expt. 4	Expt. 5	Expt. 5
T / K	1.89	1.88	1.85	1.84 K	4.34	1.74
$[CH_2OH]_0$	0.32(6)	0.3(1)	0.13(2)	0.45(2)	0.20(2)	0.34(3)
A	0.56(4)	0.88(9)	0.68(2)	0.91(2)	0.90(2)	0.95(4)
k_1 / min^{-1}	0.18(4)	0.35(6)	0.35(3)	0.35(2)	0.36(2)	0.37(3)
B	2(1)	0.49(8)	0.7(2)	0.52(6)	0.39(1)	0.5(2)
k_2 / 10^{-2} min^{-1}	1.0(4)	2.0(4)	1.3(3)	2.4(4)	1.2(8)	3(2)
C	7(30)	2.48(7)	2.4(2)	3.50(4)		8(2)
k_3 / 10^{-3} min^{-1}	1(4)	4.4(2)	3.5(4)	4.1(1)		3(1)
R^2	0.999921	0.99967	0.99971	0.999823	0.994923	0.999605

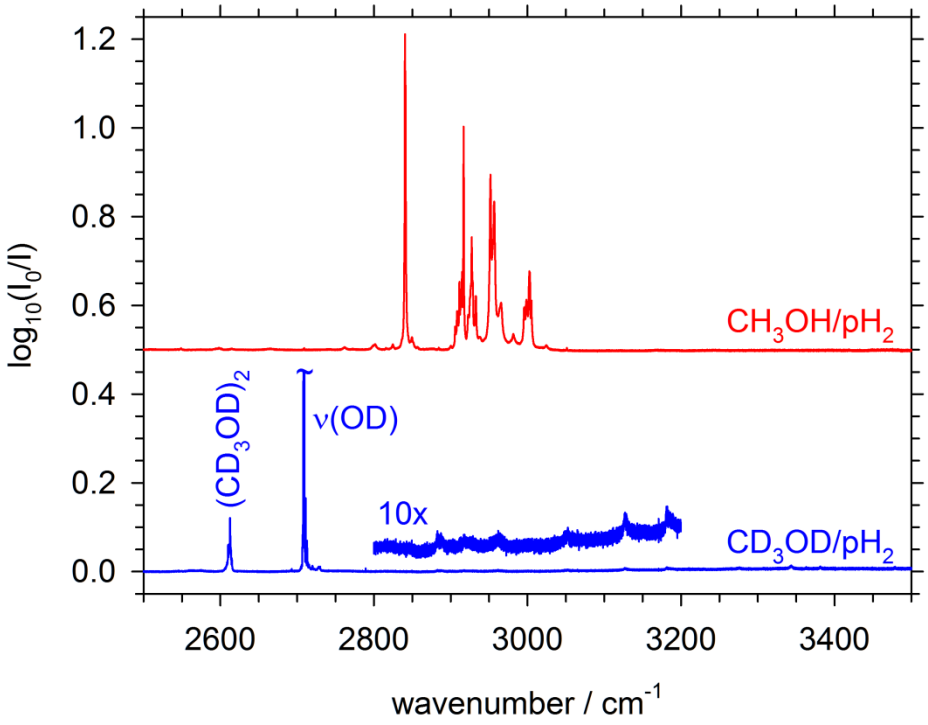

Figure S6. The observed infrared absorptions in the C-H stretching region for CD_3OD/pH_2 (blue trace) and CH_3OH/pH_2 (red trace) samples. Note the intensity of the O-D stretching peak of CD_3OD at 2709.65 cm^{-1} has been cutoff at 0.45 to allow comparison. The peak at 2612.76 cm^{-1} is due[16] to the hydrogen bonded O-D stretch of $(CD_3OD)_2$. The region from 2800 to 3200 has been magnified 10-fold to show no significant C-H stretch absorption peaks for the CD_3OD sample indicating that only minor isotopic scrambling has occurred on the carbon and the main two methanol isotopomers for the CD_3OD/pH_2 sample are CD_3OD and CD_3OH.

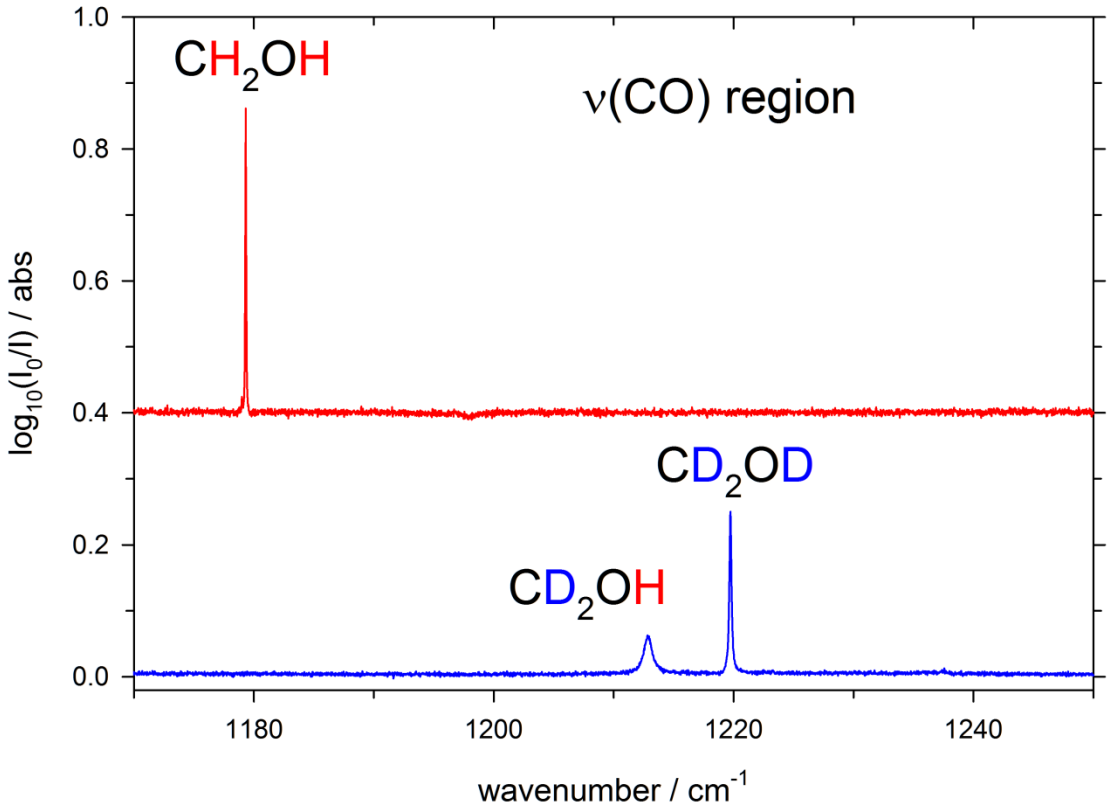

Figure S7. FTIR spectra showing the three CO stretch absorptions for CH_2OH, CD_2OH, and CD_2OD used in this study to separately monitor the hydroxymethyl isotopomer concentrations. The blue trace was recorded after photo-induced reaction of a CD_3OD/pH_2 sample (Expt. #8) and the red trace is for a CH_3OH/pH_2 sample (Expt. #5).

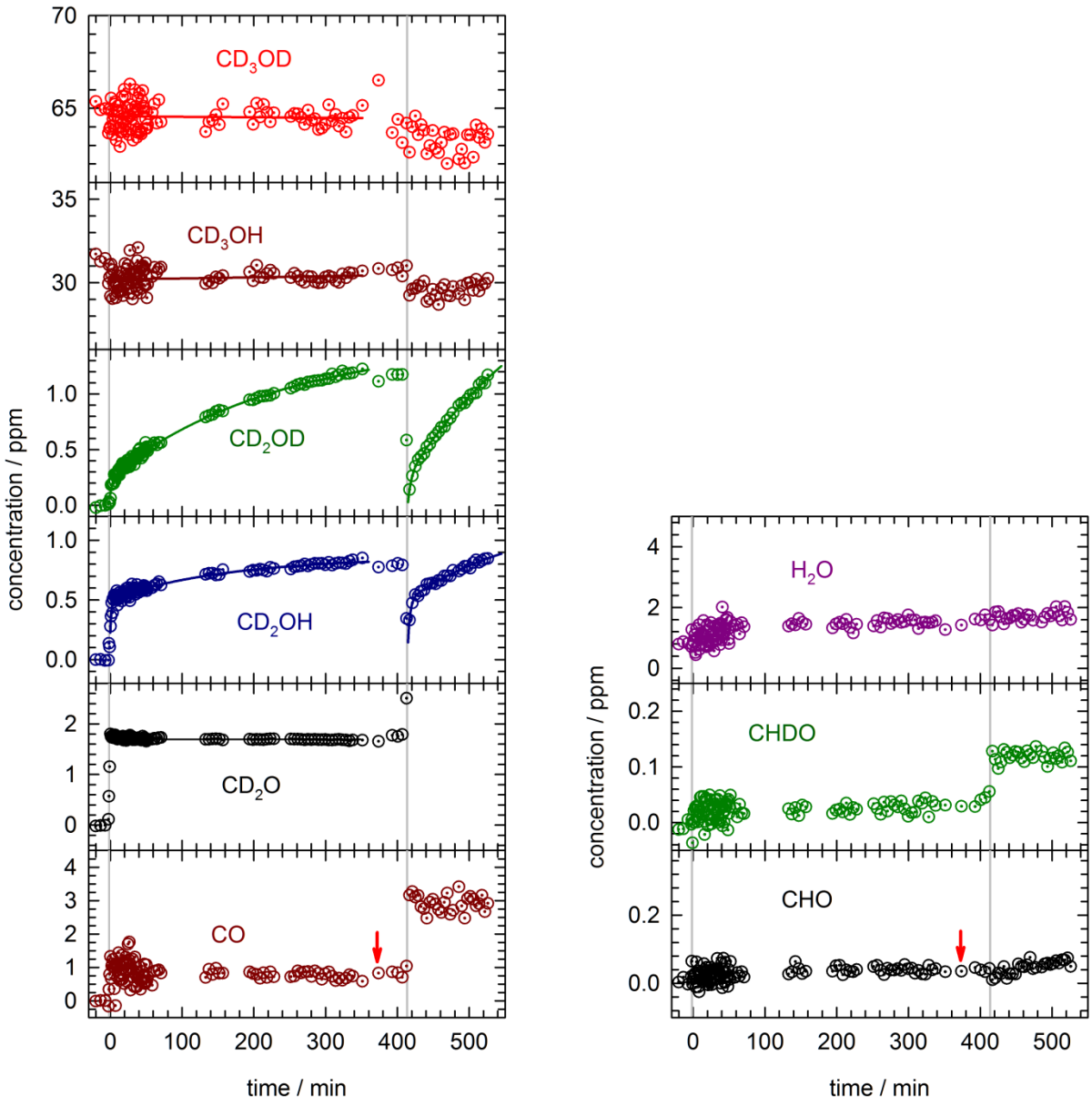

Figure S8. Full kinetic data for a low temperature photo-induced chemistry experiment conducted on an as-deposited CD_3OD/pH_2 sample (Expt. #6). Photolysis #1 consisted of a 3 min exposure (16 mW cm^{-2} at 80 Hz) and the ensuing reaction kinetics was measured at 1.89(1) K. The arrows indicate the scan recorded at 4.33 K for 10 minutes, and then the sample temperature was lowered to 1.73 K and the sample was photolyzed for a second time (3 min, 16 mW cm^{-2}, 80 Hz). The lines represent least-squares fits of the data to kinetics expressions (see text for details).

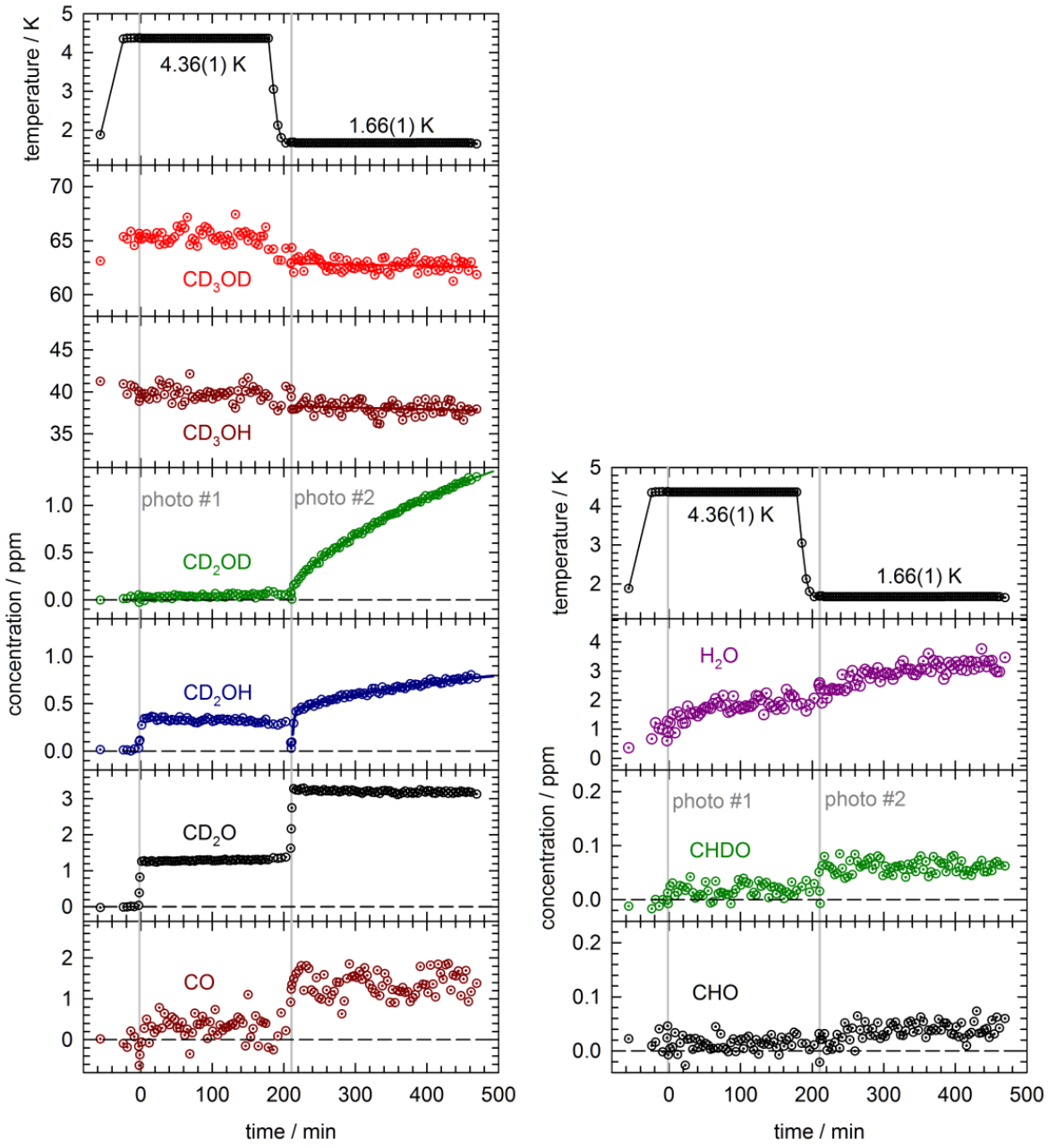

Figure S9. Kinetic data for the 193 nm photolysis (3 min, 80 Hz, 17 mW cm^{-2}) of a CD_3OD/pH_2 sample at two different temperatures (expt. #7). The first photolysis exposure (photo #1) is performed at 4.36(1) K and then the sample is cooled to 1.66(1) K and photolyzed for a second time (photo #2). The data clearly show that continued growth in CD_2OD and CD_2OH after photolysis is only observed at the lower temperature. Fits to the kinetic data are shown as color solid lines.

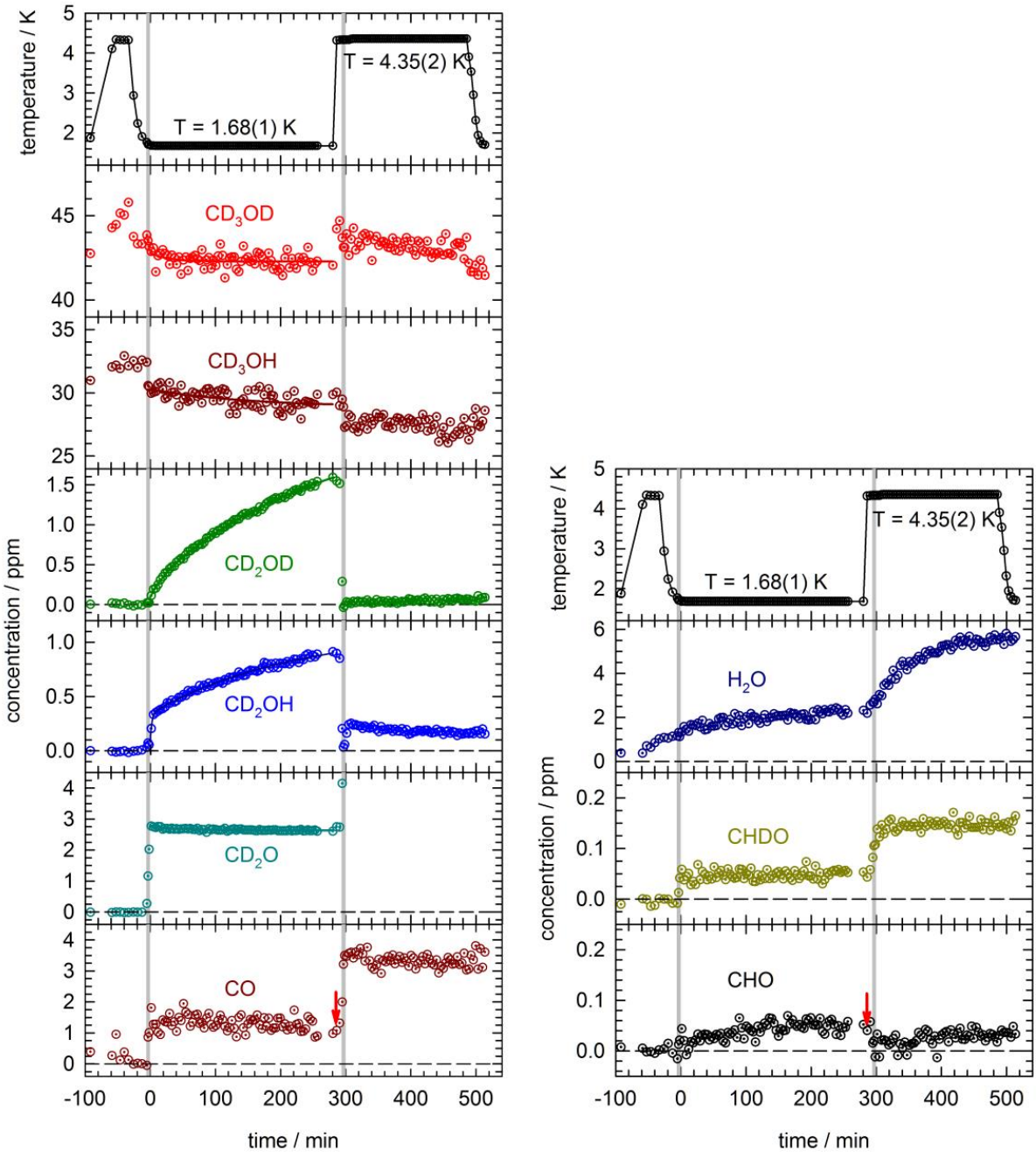

Figure S10. Kinetic data for the 193 nm photolysis (6 min, 80 Hz, 17 mW cm^{-2}) of a CD_3OD/pH_2 sample at two different temperatures (Expt. #8). The first photolysis exposure (photo #1) is performed at 1.68(1) K and then the temperature is raised to 4.35(2) K and the sample is photolyzed for a second time (photo #2). Toward the end of the second photolysis the temperature is again lowered to 1.70 K. Fits to the kinetic data are shown as color solid lines.

Table S18. Kinetic parameters for the growth of CD_2OH and CD_2OD after photolysis. All concentrations in ppm. The uncertainties in parenthesis represent the 1σ values determined from the least-squares fits of the data to the sum of two first-order expressions.

Expt. #	Expt. 6	Expt. 6	Expt. 7	Expt. 7	Expt. 8	Expt. 8
filename	KAK01161	KAK01161	KAK01169	KAK01169	KAK01177	KAK01177
T / K	1.88	1.88	1.66	1.66	1.68	1.68
species	CD_2OH	CD_2OD	CD_2OH	CD_2OD	CD_2OH	CD_2OD
$[CD_2O(H)D]_0$	0.23(3)	0.10(2)	0.18(7)	0.13(2)	0.08(7)	0.09(2)
A	0.28(3)	0.16(2)	0.26(6)	0.09(2)	0.26(7)	0.15(2)
k_1 / min^{-1}	0.6(1)	0.19(4)	0.4(1)	0.08(3)	0.4(2)	0.06(2)
B	0.35(2)	1.13(3)	0.53(5)	2.0(1)	0.77(3)	2.04(7)
k_3 / 10^{-3} min^{-1}	6.0(9)	5.6(3)	4.1(7)	3.0(3)	4.6(4)	3.9(3)
R^2	0.959858	0.995682	0.975200	0.998079	0.990050	0.998411

Table S19. Kinetic parameters for the decay of CD_3OH and CD_3OD after photolysis. All concentrations in ppm. The uncertainties in parenthesis represent the 1σ values determined from the least-squares fits of the data to Eq. (4).

Expt. #	Expt. 6	Expt. 6	Expt. 7	Expt. 7	Expt. 8	Expt. 8
filename	KAK01161	KAK01161	KAK01169	KAK01169	KAK01177	KAK01177
T / K	1.88	1.88	1.66	1.66	1.68	1.68
Species	CD_2OH	CD_2OD	CD_2OH	CD_2OD	CD_3OH	CD_3OD
$[CD_3O(H)D]_\infty$					28.9(6)	42.28(6)
A					1.4(5)	0.5(3)
k_3 /10^{-3} min^{-1}					7(6)	4(4)
R^2					0.256329	0.059282

References

(1) Lee, T. J.; Rice, J. E. Proton Affinity of Methyl Nitrate: Less than Proton Affinity of Nitric Acid. *J. Am. Chem. Soc.* **1992**, *114*, 8247-8256.

(2) Florian, J.; Leszczynski, J.; Johnson, B. G.; Goodman, L. Coupled-Cluster and Density Functional Calculations of the Molecular Structure, Infrared Spectra, Raman Spectra, and Harmonic Force Constants for Methanol. *Mol. Phys.* **1997**, *91*, 439-448.

(3) Marenich, A. V.; Boggs, J. E. A Variational Study of Nuclear Dynamics and Structural Flexibility of the CH_2OH Radical. *J. Chem. Phys.* **2003**, *119*, 3098-3105.

(4) Seidler, P.; Kongsted, J.; Christiansen, O. Calculation of Vibrational Infrared Intensities and Raman Activities Using Explicit Anharmonic Wave Functions. *J. Phys. Chem. A* **2007**, *111*, 11205-11213.

(5) Gratien, A.; Nilsson, E.; Doussin, J.-F.; Johnson, M. S.; Nielsen, C. J.; Stenstrøm, Y.; Picquet-Varrault, B. UV and IR Absorption Cross-sections of HCHO, HCDO, and DCDO. *J. Phys. Chem. A* **2007**, *111*, 11506-11513.

(6) Ruzi, M.; Anderson, D. T. Quantum Diffusion-Controlled Chemistry: Reactions of Atomic Hydrogen with Nitric Oxide in Solid Parahydrogen. *J. Phys. Chem. A* **2015**, *119*, 12270-12283.

(7) Paulson, L. O.; Mutunga, F. M.; Follett, S. E.; Anderson, D. T. Reactions of Atomic Hydrogen with Formic Acid and Carbon Monoxide in Solid Parahydrogen I: Anomalous Effect of Temperature *J. Phys. Chem. A* **2014**, *118*, 7640-7652.

(8) Lee, Y.-F.; Chou, W.-T.; Johnson, B. A.; Tabor, D. P.; Sibert III, E. L.; Lee, Y.-P. Infrared Absorption of CH_3O and CD_3O Radicals Isolated in Solid para-H_2. *J. Mol. Spectrosc.* **2015**, *310*, 57-67.

(9) Lee, Y.-F.; Kong, L.-J.; Lee, Y.-P. Infrared Absorption of CH_3OSO and CD_3OSO Radicals Produced Upon Photolysis of $CH_3OS(O)Cl$ and $CD_3OS(O)Cl$ in *p*-H_2 Matrices. *J. Chem. Phys.* **2012**, *136*, 124510-8.

(10) Feng, L.; Wei, J.; Reisler, H. Rotationally Resolved Infrared Spectroscopy of the Hydroxymethyl Radical (CH_2OH). *J. Phys. Chem. A* **2004**, *108*, 7903-7908.

(11) Roberts, M. A.; Sharp-Williams, E. N.; Nesbitt, D. J. High-Resolution Direct-Absorption Spectroscopy of Hydroxymethyl Radical in the CH Symmetric Stretching Region. *J. Phys. Chem. A* **2013**, *117*, 7042-7049.

(12) Johnson III, R. D.; Hudgens, J. W. Structural and Thermochemical Properties of Hydroxymethyl (CH_2OH) Radicals and Cations Derived from Observations of B $^2A'(3p) \leftarrow X\ ^2A''$ Electronic Spectra and from Ab Initio Calculations. *J. Phys. Chem.* **1996**, *100*, 19874-19890.

(13) Jacox, M. E.; Milligan, D. E. Matrix Isolation Study of the Vacuum-Ultraviolet Photolysis of Methanol. *J. Mol. Spectrosc.* **1973**, *47*, 148-162.

(14) Jacox, M. E. The Reaction of excited Argon Atoms and of F Atoms with Methanol. Vibrational Spectrum of CH_2OH Isolated in Solid Argon. *Chem. Phys.* **1981**, *59*, 213-230.

(15) Cheng, B.-M.; Bahou, M.; Chen, W.-C.; Yui, C.-h.; Lee, Y.-P.; Lee, L. C. Experimental and theoretical studies on vacuum ultraviolet absorption cross sections and photodissociation of CH_3OH , CH_3OD , CD_3OH , and CD_3OD. *J. Chem. Phys.* **2002**, *117*, 1633-1640.

(16) Larsen, R. W.; Zielke, P.; Suhm, M. A. Hydrogen-Bonded OH Stretching Modes of Methanol Clusters: A Combined IR and Raman Isotopomer Study. *J. Chem. Phys.* **2007**, *126*, 194307-18.